This paper describes objective technical results and analysis. Any subjective views or opinions that might be expressed in the paper do not necessarily represent the views of the U.S. Department of Energy or the United States Government.

SAND2021-4593C
Proceedings of the ASME 2021
Pressure Vessels & Piping Conference
PVP 2021
July 12-16, 2021, Virtual, Online

PVP2021-62944

EFFECT OF INTERNAL HYDROGEN ON FATIGUE CRACK INITIATION SITES IN 316L AUSTENITIC STAINLESS STEEL

B. Kagay, J. Ronevich, C. San Marchi
Sandia National Laboratories
Livermore, CA, USA

ABSTRACT

Internal hydrogen can influence the fatigue life, crack growth rate, and crack morphology of austenitic stainless steel, but little is known about the effect of internal hydrogen on fatigue crack initiation sites. To determine the effect of internal hydrogen on the microstructural fatigue crack initiation sites, the location of small fatigue cracks was evaluated with respect to the microstructural features in notched middle tension M(T) 316L specimens both with and without pre-charged hydrogen. The notches of the M(T) specimens were electropolished prior to fatigue testing to facilitate post-test analysis. Fatigue tests were performed with the same constant load amplitude and an R-ratio of 0.1 for specimens with and without internal hydrogen. The fatigue tests were interrupted after a minimal amount of cracking was detected using the direct current potential difference (DCPD) technique. The microstructural locations of the small fatigue cracks were then evaluated with scanning electron microscopy imaging and electron backscatter diffraction (EBSD). Several small transgranular fatigue cracks initiated in the notches of specimens both with and without internal hydrogen. These transgranular cracks always intersected grain boundaries, twin boundaries, and/or triple points indicating that these microstructural features are the critical locations for crack initiation. The transgranular cracks did not propagate along the prominent slip traces. There was no discernible effect of hydrogen on the microstructural sites of fatigue crack initiation in 316L.

INTRODUCTION

Pressure cycling of high-pressure hydrogen systems results in large cyclic stresses in these components, which are often produced from austenitic stainless steels, such as type 316 and type 316L. Hydrogen absorption coupled with cyclic loading has the potential to enhance fatigue failures of these high-pressure hydrogen components due to hydrogen embrittlement phenomena.

Hydrogen has been shown to decrease the fatigue life [1–3] and increase the fatigue crack growth rate [4–7] of austenitic stainless steels, but there have been few studies on the effects of hydrogen on fatigue crack initiation [7–9]. In particular, the influence of hydrogen on the microstructural sites for fatigue crack initiation in austenitic stainless steels is unknown. An understanding of the relationship between microstructure and fatigue crack initiation may enable microstructural design to improve fatigue life in hydrogen environments.

In this study, the effects of internal hydrogen on the fatigue crack initiation microstructural sites of 316L stainless steel are evaluated through interrupted fatigue testing of middle tension M(T) specimens with and without internal precharged hydrogen. The DCPD technique is used to interrupt tests when only small cracks have formed and then the location of the small cracks in the microstructure are determined with scanning electron microscopy and electron backscatter diffraction (EBSD). The initiation and propagation of the small cracks in the notches of the 316L specimens are discussed with respect to the plastic deformation.

EXPERIMENTAL PROCEDURES

316L rolled bar with the composition shown in Table 1 was evaluated. Tensile specimens were extracted from the bar with the tensile direction of the specimen in the radial direction of the bar, and the center of the gauge length of the tensile specimens centered in the middle of the bar. The cylindrical specimens had a gauge diameter of approximately 2.87 mm. Tensile testing was performed at a strain rate of 3.33×10^{-4} s^{-1} and with a 12.7 mm (0.5 in) extensometer to measure elongation. All tensile and fatigue tests were performed on a servohydraulic load frame.

M(T) specimens were machined from the rolled bar with both the loading direction and the crack growth directions in the radial direction of the bar and with the holes of the M(T) specimens centered in the bar. The dimensions of the M(T) specimens are provided in Figure 1. The K_t of the M(T) specimens is 3.9. Prior to fatigue testing, the notches of the M(T)

© 2021 by ASME

Sandia National Laboratories is a multimission laboratory managed and operated by National Technology & Engineering Solutions of Sandia, LLC, a wholly owned subsidiary of Honeywell International Inc., for the U.S. Department of Energy's National Nuclear Security Administration under contract DE-NA0003525.

specimens were electropolished so that EBSD could be performed after testing without additional preparation. Load-control tension-tension fatigue testing was performed with maximum loads of 3.781 kN and 4.893 kN with an R-ratio of 0.1 and a frequency of 1 Hz. These loads correspond to nominal stresses of 280 and 360 MPa, respectively.

Tensile and fatigue testing was performed on 316L specimens without internal hydrogen (as-received (AR)) and with internal hydrogen (H-precharged (PC)) in the ambient laboratory environment (temperature of approximately 20°C). Thermal precharging in gaseous hydrogen at a pressure of 138 MPa and a temperature of 300°C for at least 10 days results in a uniform concentration of approximately 140 wt. ppm internal hydrogen in the specimens [10]. After precharging the specimens were stored in a freezer at −50°C (223K) to prevent hydrogen egress.

The DCPD method was utilized to identify crack initiation and to interrupt the tests when a minimal amount of cracking had occurred. A constant current of 1 A was applied across the length of the specimen through two wires spot-welded about 15 mm away from the notch on opposite faces of the specimen. A high sensitivity to crack initiation was achieved by spot welding separate voltage leads for each notch of the M(T) specimen. The wires for each notch were welded to opposite faces of the specimen as shown in Figure 1(b). In order to minimize thermoelectric effects, the direction of current flow was reversed every 5 s. The number of cycles to crack initiation was selected as the inflection point at which the DCPD voltage signal began to continuously increase.

Scanning electron imaging and EBSD was performed with a FEI Helios Nanolab Dualbeam FIB/SEM. The MT specimens were tilted to an angle of 70° between the normal to the center of the notch and the electron beam. For EBSD an accelerating voltage of 25 keV and step sizes of 0.1 µm, 0.2 µm, or 0.5 µm were used. The SEM images were captured with the Everhart-Thornley detector and were tilt-corrected. For each specimen, cracks were identified and imaged for one of the two notches.

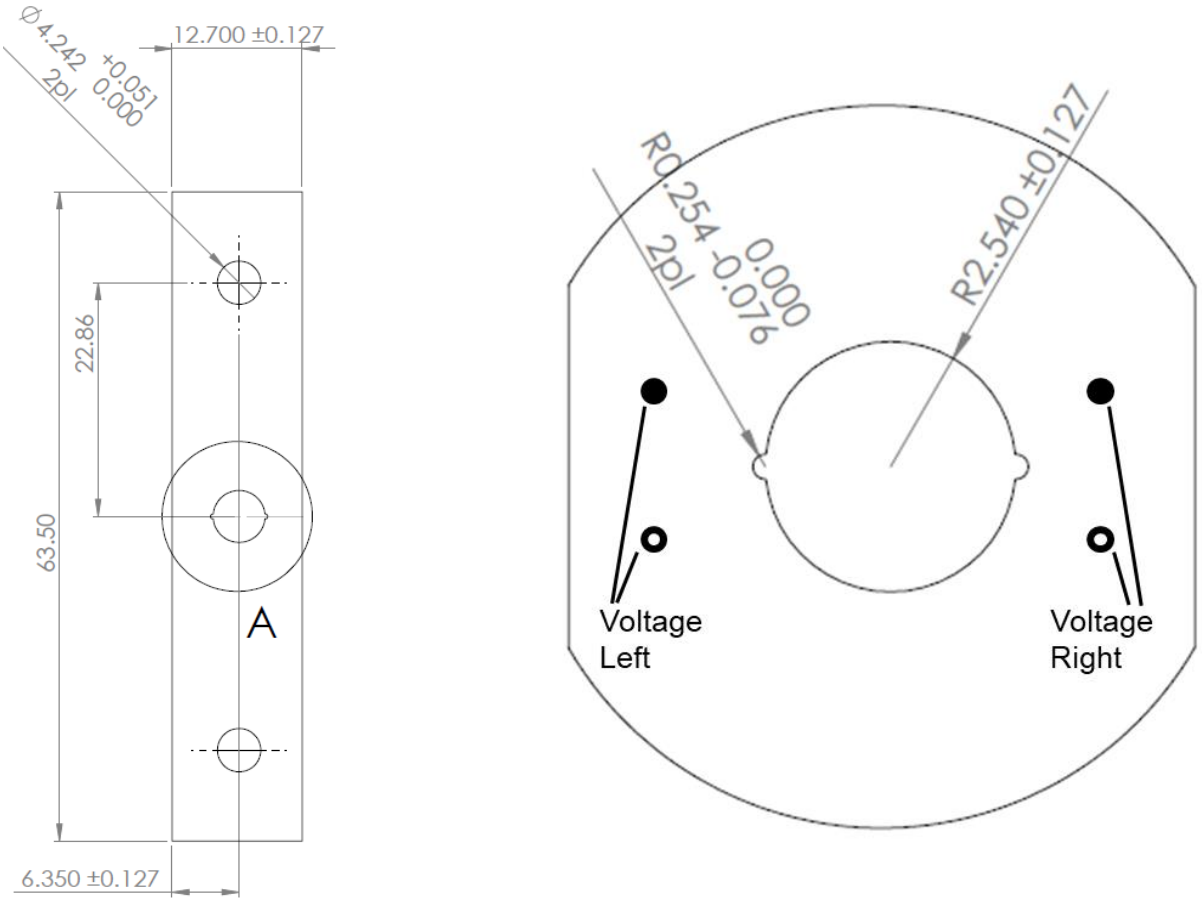

(a) **(b)**

Figure 1 (a) M(T) specimen drawing and (b) detail of notch with locations of DCPD voltage leads. All dimensions are in mm.

© 2021 by ASME

Table 1 – Composition of 316L Bar

wt %	Cr	Ni	Mn	Mo	C	N	Si	S	P	Cu	Fe
316L Bar	17.57	12.97	1.25	2.71	0.017	0.048	0.59	0.009	0.022	0.22	Bal.

RESULTS

The tensile properties of the 316L bar in the as-received (AR) and hydrogen precharged (PC) states are provided in Table 2. Pre-charged hydrogen increased the yield stress and ultimate tensile stress (UTS) and decreased the uniform elongation, total elongation, and reduction of area of the 316L bar.

The condition (AR or PC), maximum applied cyclic stress (S_{max}), cycles to crack initiation from DCPD (N_i), and the number of cycles at which each test was stopped (N Interrupt) are given in Table 3. Crack initiation occurred at a greater number of cycles for the PC condition than the AR condition for both stress levels. A plot of the normalized maximum stress (Smax/UTS) versus the cycles to crack initiation is shown for the AR and PC conditions in Figure 2. The AR and PC conditions show a similar trend in Figure 2, which indicates that the greater number of cycles to crack initiation for the PC condition than the AR condition for a given applied stress is likely due to the increase in strength from internal hydrogen for the PC condition.

A total of 12 cracks for the AR condition and 9 cracks for the PC condition were identified and imaged from the combination of 4 tested specimens. Multiple cracks were observed in the notch of each specimen, and these cracks were dispersed along the notch. The surface cracks ranged from 5 μm in length to 200 μm. Examples of the cracks found in the notches of the M(T) specimens are shown in the scanning electron micrographs and inverse pole figure (IPF) maps in Figure 3-5. For all images in Figures 2-5, the loading direction is horizontal and the IPF map is for the normal direction. In the scanning electron micrographs for all cracks, slip bands are visible with extrusions and intrusions present at many of the slip bands. No distinct difference in the crack initiation location or crack propagation mode could be determined for the AR and PC conditions; as such, the following observations apply to both conditions.

Every crack intersected or propagated less than 2 microns away from a grain boundary, twin boundary, or triple point. Examples of cracks intersecting a triple point are circled for the AR condition in Figure 3 and for the PC condition in Figure 4 and Figure 5. The triple points in Figure 3 and Figure 4 contain one twin boundary, while the triple point in Figure 5 contains three general grain boundaries. The crack in Figure 6 for the AR condition propagates along the intersection of two twin boundaries. No cracks wholly contained within the middle of a grain were observed.

Crack propagation was almost entirely transgranular and not along the prominent slip bands. Transgranular crack propagation crossing the extrusions and intrusions is evident in Figures 2-5. The long transgranular cracks in Figure 3 likely initiated at the triple point before emanating into the adjacent grains. Only small excursions along slip bands, grain boundaries, and twin boundaries could be observed. A small portion of a crack along a slip band and twin boundary for a specimen in the AR condition is circled in Figure 6. The crack in Figure 6 extends up and to the left and down and to the right away from the twin boundary and terminates at primary slip bands.

Crack propagation was sometimes observed to occur along the edge of regions where a second set of slip bands were visible along with a more prominent set of slip bands. In Figure 4 and Figure 5, the cracks appear to be encircling regions containing a second set of slip bands which are finer spaced and less prominent than the primary slip bands. The crack in Figure 6 propagates between two of the primary slip bands and along the edges of the smaller slip bands. One crack for each condition was also observed to intersect an inclusion. No strain-induced α'-martensite was observed.

Table 2 – Tensile Properties of As-Received (AR) and Hydrogen Pre-Charged (PC) 316L Bar

	Condition	0.2% Yield Stress (MPa)	UTS (MPa)	Uniform Elongation (%)	Total Elongation (%)	Reduction of Area (%)
316L Bar	AR	487	638	33.8	46.1	50.6
316L Bar	PC	563	681	24.7	32.2	33.6

Table 3 – S_{max}, Cycles to Initiation, and Cycles to Interruption for Fatigue Tests

Condition	S_{max} (MPa)	N_i	N Interrupt
AR	278	13,300	23,875
AR	361	3,800	6,983
PC	280	19,500	24,598
PC	361	4,800	10,992

© 2021 by ASME

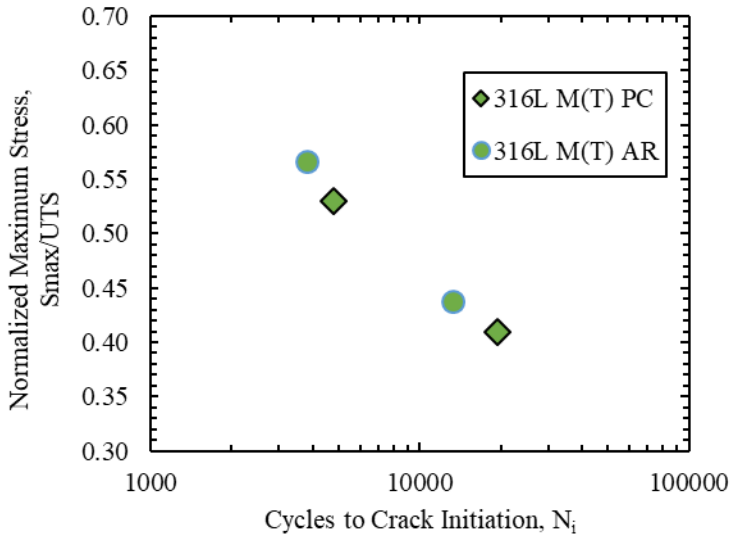

Figure 2 Maximum applied stress normalized by the ultimate tensile stress (S_{max}/UTS) versus cycles to crack initiation for the 316L M(T) specimens in the AR and PC conditions.

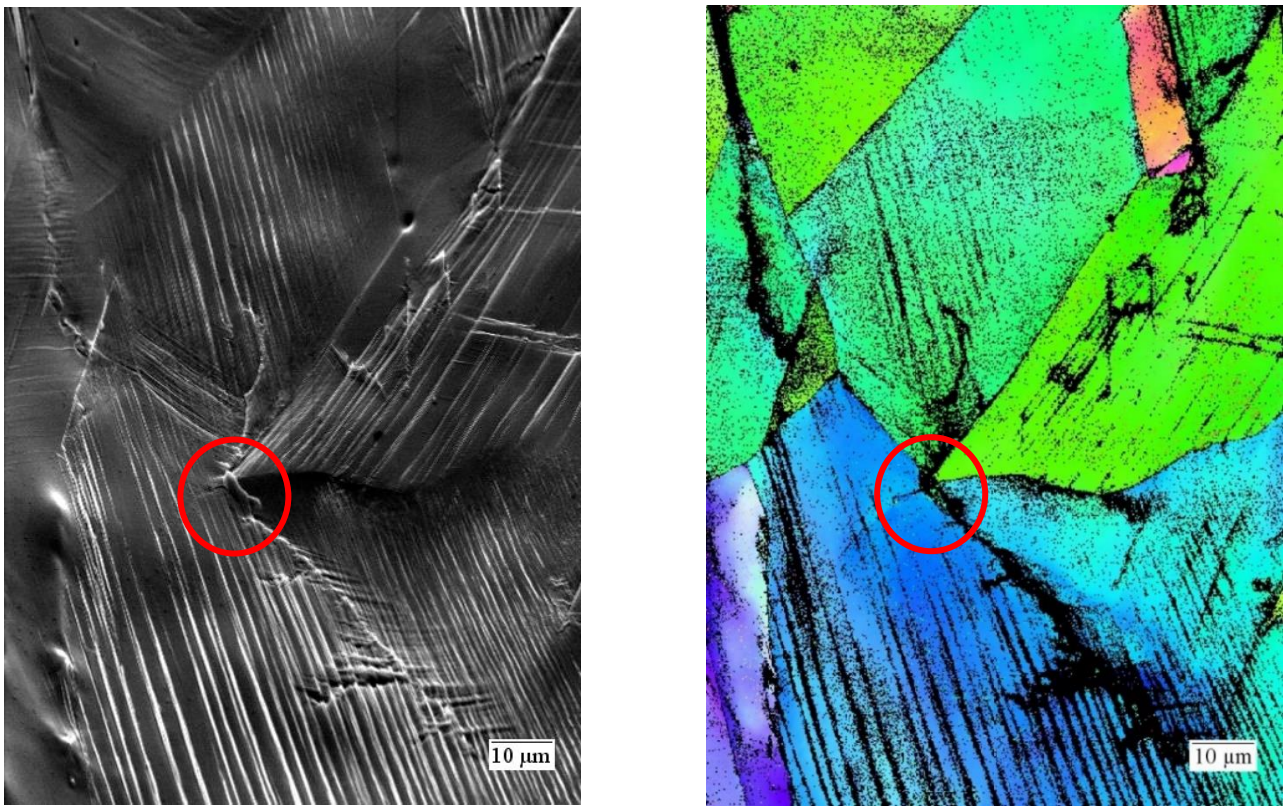

(a) **(b)**

Figure 3 (a) Scanning electron micrograph and (b) IPF map of a crack in a AR M(T) specimen tested with P_{max} = 361 MPa. Loading direction is horizontal. IPF map for normal-direction. Step size of 0.2 µm.

© 2021 by ASME

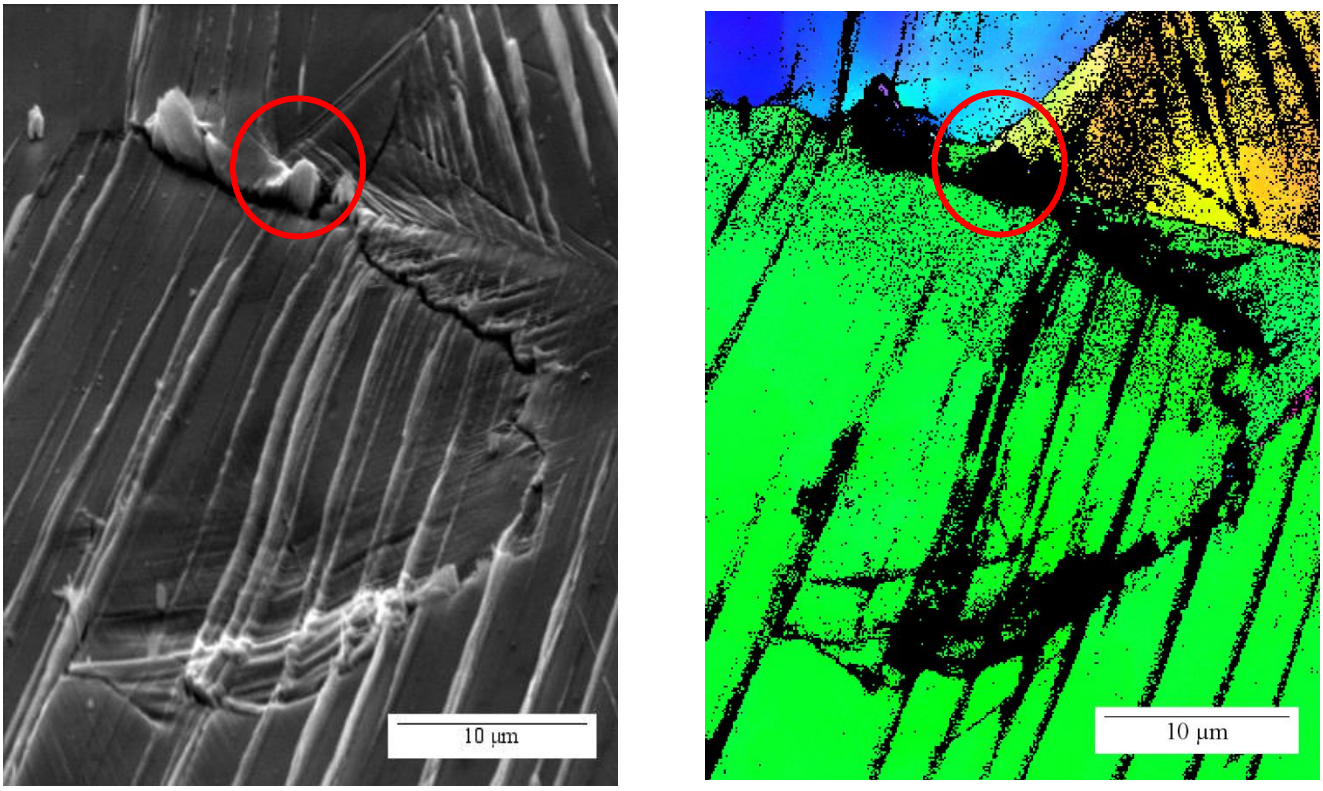

(a) (b)

Figure 4 (a) Scanning electron micrograph and (b) IPF map of a crack in a PC M(T) specimen tested with P_{max} = 361 MPa. Loading direction is horizontal. IPF map for normal-direction. Step size of 0.1 µm.

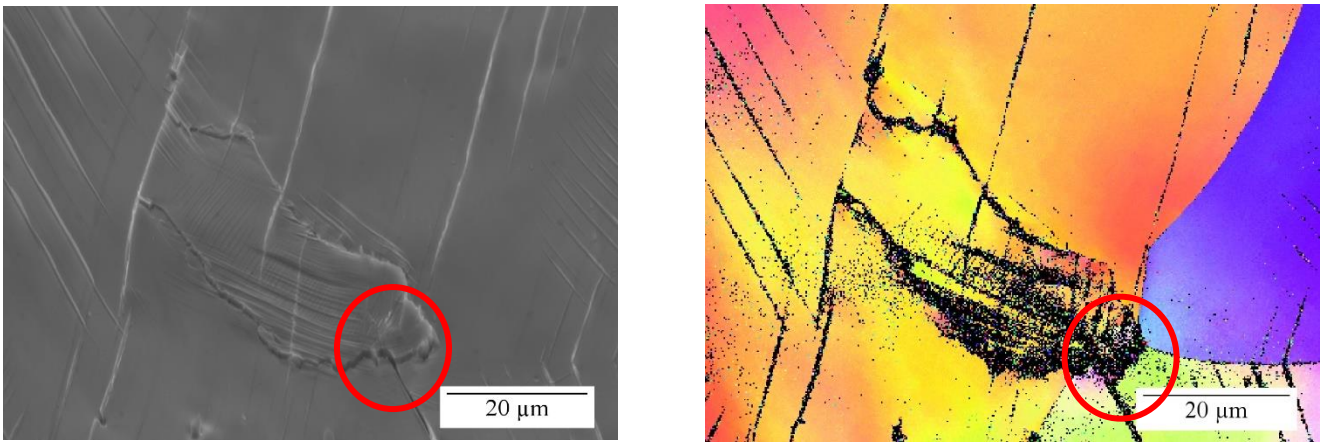

(a) (b)

Figure 5 (a) Scanning electron micrograph and (b) IPF map of a crack in a PC M(T) specimen tested with P_{max} = 279 MPa. Loading direction is horizontal. IPF map for normal-direction. Step size of 0.2 µm.

© 2021 by ASME

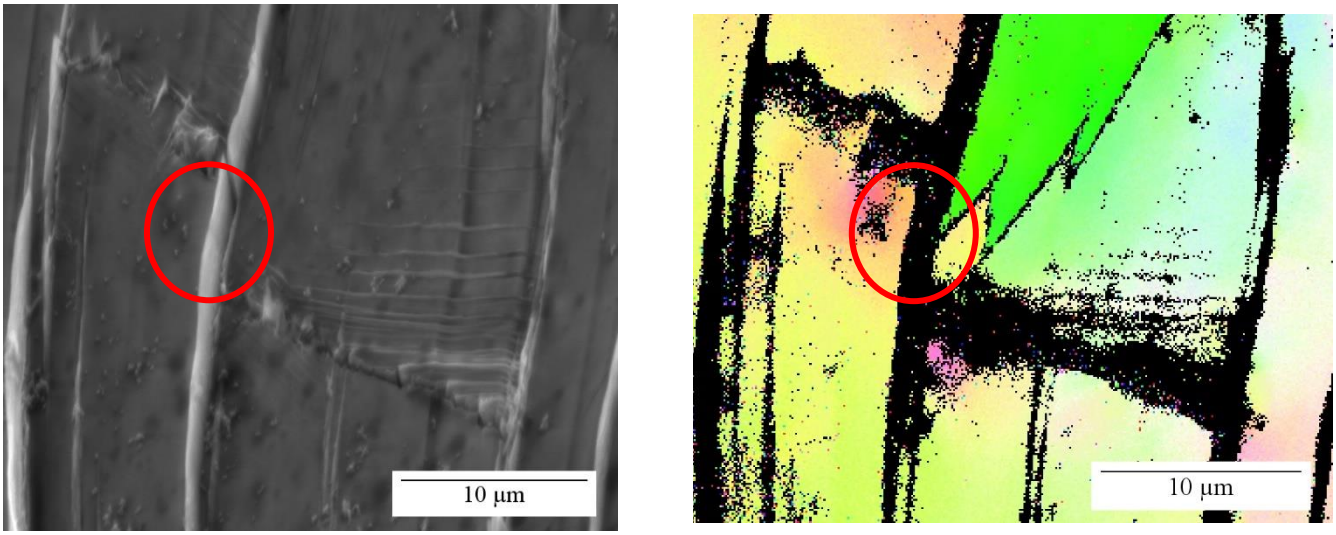

(a) **(b)**

Figure 6 (a) Scanning electron micrograph and (b) IPF map of a crack in a AR M(T) specimen tested with P_{max} = 279 MPa. Loading direction is horizontal. IPF map for normal-direction. Step size of 0.1 µm.

DISCUSSION

The microstructural crack initiation sites and crack propagation modes in 316L were not changed by internal hydrogen. Internal hydrogen does not appear to activate any particular microstructural site for fatigue crack initiation and short crack propagation in 316L. The initiation lifetimes, for example, fall along the same trend line for both conditions if the relative stress is taken into account (since precharging increases the strength of the material), as can be seen in Figure 2. Moreover, internal hydrogen does not change the morphology of the cracks with respect to the microstructure, as shown in Figures 3-6. Effects of internal hydrogen on fatigue crack initiation and short crack growth rates for 316L appear to be due to hydrogen enhancing the same crack initiation and propagation mechanisms that occur in inert environments.

Since all cracks intersected or were located directly next to grain boundaries or triple points, these appear to be the critical locations for fatigue crack initiation in this material (both without and with internal hydrogen). Grain boundaries and triple points may function as an obstacle to dislocation motion resulting in dislocation pile-ups that increase the local stress and result in microcrack initiation. Microcracks may initiate at the boundaries or within the dislocation pile-ups adjacent to the boundaries.

Several other studies have evaluated the microstructural location of fatigue crack initiation in 316L [11–16] and 304L [17]. In addition to cracks that initiated at grain boundaries, triple points, and inclusions, those studies observed cracks that initiated and propagated along slip bands and twin boundaries. There are several possible explanations for the lack of slip band and twin boundary cracking observed in this study. Slip band cracking may be more likely to occur when primarily single slip occurs since deformation will be localized to only one set of slip bands. Previous studies have been performed with smooth specimens, where the uniform stress state and low stresses may limit the activation of multiple slip systems. In contrast, the stress state is more complicated, and the stresses are larger at the notch of the M(T) specimens, which may result in more active slip systems. Higher stresses at the notches of the M(T) specimens compared to smooth specimens in other studies is also indicated by the relatively low cycles to crack initiation for the M(T) specimens (less than 10,000 cycles). Additionally, strain-hardened 316L was used in this study while most studies have been performed with annealed 316L. The additional dislocations present in the strain-hardened material may act as barriers to dislocation motion on the primary slip planes with the highest Schmid factor. Dislocation pile-ups may then occur on the primary slip bands at lower amounts of strain and result in activation of secondary slip systems. On the other hand, one other study of cold-rolled 316L did observe crack initiation and propagation at both slip bands and twin boundaries [11].

Cracks along the edge of regions with a second set of slip bands indicates that multiple active slip systems may play a critical role in propagation of short fatigue cracks in 316L. Microcracks initiated at grain boundaries and triple points may raise the local stress causing more dislocation motion on secondary slip systems. Consequently, dislocation cells may form at the intersection of those slip systems where dislocation motion is blocked, and the crack may propagate preferentially where the dislocation cells have formed.

© 2021 by ASME

CONCLUSIONS

The microstructural fatigue crack initiation and propagation sites of strain-hardened 316L with and without internal hydrogen were evaluated through scanning electron microscopy and EBSD. Fatigue tests of electropolished M(T) specimens were interrupted after crack initiation had been identified with the DCPD technique. Internal hydrogen did not change the microstructural crack initiation sites or crack propagation modes of 316L. Cracks appeared to initiate at grain boundaries, twin boundaries, and triple points. Crack propagation was transgranular and did not follow the prominent slip bands. Significant grain boundary and twin boundary crack propagation was also not observed. Internal hydrogen may influence the dislocation motion and accumulation leading to fatigue crack initiation and propagation but does not appear to specifically activate different microstructural sites.

ACKNOWLEDGEMENTS

The authors gratefully acknowledge assistance from J.A. Campbell for hydrogen pressure systems support. We also acknowledge the funding support of the Energy Efficiency and Renewable Energy Office's Hydrogen and Fuel Cell Technologies Office at the U.S. Department of Energy. Sandia National Laboratories is a multimission laboratory managed and operated by National Technology and Engineering Solutions of Sandia, LLC., a wholly owned subsidiary of Honeywell International, Inc., for the U.S. Department of Energy's National Nuclear Security Administration under contract DE-NA-0003525. This paper describes objective technical results and analysis. Any subjective views or opinions that might be expressed in the paper do not necessarily represent the views of the U.S. Department of Energy or the United States Government.

REFERENCES

1 P. J. Gibbs, C. San Marchi, K. A. Nibur, and X. Tang, "Comparison of Internal and External Hydrogen on Fatigue-Life of Austenitic Stainless Steels," *(paper no. PVP2016-63563), ASME Pressure Vessels and Piping Division Conference, 17-21 July 2016, Vancouver, Canada*.

2 C. San Marchi, J. Yamabe, M. Schwarz, H. Matsunaga, S. Zickler, S. Matsuoka, and H. Kobayashi, "Global Harmonization of Fatigue Life Testing in Gaseous Hydrogen," (paper no. *PVP2018-84898), ASME Pressure Vessels and Piping Division Conference, 15-20 July 2018, Prague, Czech Republic*.

3 C. San Marchi, P. Gibbs, J. Foulk, and K. Nibur, "Fatigue Life of Austenitic Stainless Steel in Hydrogen Environments," in *43rd MPA Seminar*, 2017.

4 T. R. Smith, C. S. Marchi, J. D. Sugar, and D. K. Balch, "Effects of extreme hydrogen environments on the fracture and fatigue behavior of additively manufactured stainless steels," (paper no. PVP2019-93903), *ASME Pressure Vessels and Piping Division Conference, 14-19 July 2019, San Antonio, TX*.

5 Y. Ogawa, S. Okazaki, O. Takakuwa, and H. Matsunaga, "The roles of internal and external hydrogen in the deformation and fracture processes at the fatigue crack tip zone of metastable austenitic stainless steels," *Scr. Mater.*, vol. 157, pp. 95–99, 2018.

6 X. Chen, C. Zhou, J. Zheng, and L. Zhang, "Effects of a ′ martensite and deformation twin on hydrogen-assisted fatigue crack growth in cold / warm-rolled type 304 stainless steel," *Int. J. Hydrogen Energy*, vol. 43, no. 6, pp. 3342–3352, 2018.

7 K. A. Nibur, P. J. Gibbs, J. W. Foulk, and C. San Marchi, "Notched Fatigue of Austentic Alloys in Gaseous Hydrogen," *(paper no. PVP2017-65978), ASME Pressure Vessels and Piping Division Conference, 16-20 July 2017, Waikoloa, Hawaii.*.

8 Y. Murakami, T. Kanezaki, and Y. Mine, "Hydrogen Effect against Hydrogen Embrittlement," *Metall. Mater. Trans. A Phys. Metall. Mater. Sci.*, vol. 41, no. 10, pp. 2548–2562, 2010.

9 B. Kagay, C. San Marchi, V. Pericoli, and J. Foulk, "Hydrogen effects on fatigue life of welded austenitic stainless steels evaluated with hole-drilled tubular specimens," *(paper no. PVP2020-8576), ASME Pressure Vessels and Piping Division Conference, 2020.*

10 C. San Marchi, B. P. Somerday, X. Tang, and G. H. Schiroky, "Effects of alloy composition and strain hardening on tensile fracture of hydrogen-precharged type 316 stainless steels," *Int. J. Hydrogen Energy*, vol. 33, no. 2, pp. 889–904, 2008.

11 M. D. Roach, S. I. Wright, J. E. Lemons, and L. D. Zardiackas, "An EBSD based comparison of the fatigue crack initiation mechanisms of nickel and nitrogen-stabilized cold-worked austenitic stainless steels," *Mater. Sci. Eng. A*, vol. 586, pp. 382–391, 2013.

12 M. Kamaya, "Influence of bulk damage on crack initiation in low-cycle fatigue of 316 stainless steel," *Fatigue Fract. Eng. Mater. Struct.*, vol. 33, pp. 94–104, 2009.

13 U. Lindstedt, B. Karlsson, and M. Nystrom, "Small Fatigue Cracks in an Austenitic Stainless Steel," *Fatigue Fract. Eng. Mater. Struct.*, vol. 21, pp. 85–98, 1998.

14 J. Polák, J. Man, T. Vystavˇ, and M. Petrenec, "The shape of extrusions and intrusions and initiation of stage I fatigue cracks," *Mater. Sci. Eng. A*, vol. 517, pp. 204–211, 2009.

15 P. Mu, V. Aubin, I. Alvarez-armas, and A. Armas, "Influence of the crystalline orientations on microcrack initiation in low-cycle fatigue," *Mater. Sci. Eng. A*, vol. 573, pp. 45–53, 2013.

16 L. Signor, P. Villechaise, T. Ghidossi, E. Lacoste, M. Gueguen, and S. Courtin, "Influence of local crystallographic configuration on microcrack initiation in fatigued 316LN stainless steel: Experiments and crystal plasticity finite elements simulations," *Mater. Sci. Eng. A*, vol. 649, pp. 239–249, 2016.

17 J. W. Pegues, M. D. Roach, and N. Shamsaei, "Influence of microstructure on fatigue crack nucleation and microstructurally short crack growth of an austenitic stainless steel," *Mater. Sci. Eng. A*, vol. 707, pp. 657–667, 2017.

 © 2021 by ASME